ANALYSIS AND TEST OF GUN BLAST RESISTANT COMPOSITE STRUCTURE

Dennis K. McCarthy

The Boeing Company
5000 East McDowell
Mesa, Arizona 85215

ABSTRACT

The lower skins on the Extended Forward Avionics Bay (EFAB) on the AH-64D Apache are exposed to muzzle blast effects from a belly mounted 30 mm chain gun. These composite skins must be sufficiently strong to withstand blast pressure at a minimum weight. Analytical methods presented predict behavior of structure subject to gun muzzle blast. This resulted in a weight-optimized, blast-resistant EFAB design which was fabricated and attached to an aircraft. The chain gun was fired near these skins during hover and forward flight without structural damage. Strain data collected during gun fire verified the analytical method.

INTRODUCTION

The AH-64 Apache attack helicopter is equipped with a 30mm Chain Gun® automatic cannon on the lower forward fuselage as shown in Figure 1. The chain gun pivots left and right (azimuth) and up and down (elevation) for targeting. At certain azimuths and elevations the gun muzzle is in close proximity to the lower skins on the Extended Forward Avionics Bay (EFAB). The proximity of the gun and EFAB's is shown in Figure 2.

On the A-Model Apache FAB's various aluminum skin configurations were tried until no muzzle blast failures occurred. Although this trial and error method resulted in a satisfactory design it was costly and time consuming. The Extended Forward Avionics Bays (EFAB) on the D-Model Longbow Apache were designed using carbon fiber reinforced plastic (CFRP). Rather than using trial and error, analytical methods based on prior work [1,2, and 3] were developed and analysis was performed to predict Longbow EFAB skin behavior subjected to gun muzzle blast.

In this analysis method structure is modeled using a finite element mesh. Gun muzzle blasts are simulated using a blast model from the Naval Ordnance Laboratory (NOL) [4,5] and pressure characteristics of the 30mm gun. Using these analytical methods the EFAB structure was optimized to minimize weight without structural damage from gun muzzle blast.

Figure 1. AH-64D Apache Longbow With 30mm Chain Gun® Automatic Cannon

Figure 2. AH-64D Apache with Extended Forward Avionics Bay

The EFABs were fabricated based on the optimized design and attached to an aircraft. A strain gage rosette was placed on the inside center of one bay of the left lower EFAB skin. The 30mm cannon was then fired repeatedly during hover and forward flight at an azimuth and elevation exposing the left lower EFAB skin to maximum muzzle blast pressure. Strain data from the rosette was compared with that from the analysis method with good agreement.

GUN MUZZLE BLAST CHARACTERISTICS

Gun blast is a shock wave traveling away from the muzzle. As this wave contacts structure it subjects the structure to a rapid increase followed by a slower decrease in pressure. This pressure wave is shown at an instant in time in Figure 3.

Ahead of the front of the shock wave, shown as an expanding sphere, the structure is subjected to ambient pressure. Immediately behind the wave front the panel is subjected to the ring shaped pressure profile shown. Inside the trailing edge of the shock wave the structure is once again subjected to ambient pressure.

A representative blast pressure wave is shown at various times in Figure 4. At 100 and 200 μs the expanding shock wave has yet to reach the panel. At 300 μs the shock wave has hit the panel and the resulting pressure profile is shown. From 300 to 375 μs, maximum pressure decreases as the front of the shock wave travels across the panel. At 400 μs the shock wave has passed the center of the panel resulting in the ring shaped profile shown. From 400 μs on the pressure ring progresses across the panel continually decreasing in pressure.

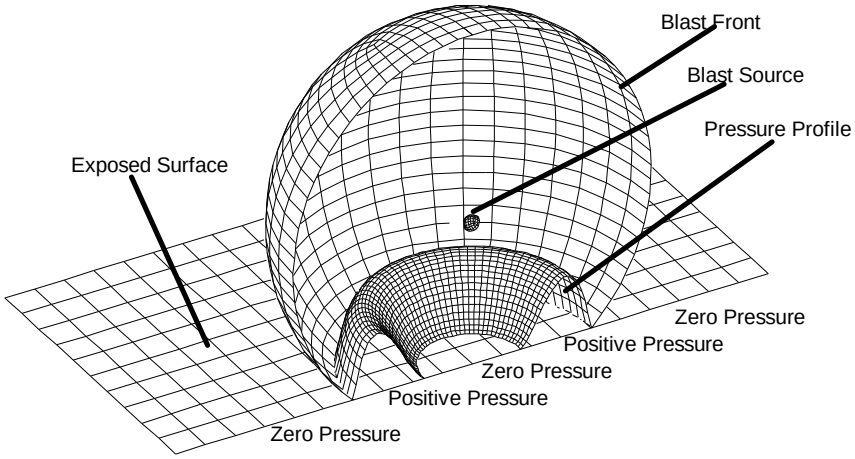

Figure 3. Gun Blast Pressure Wave Details

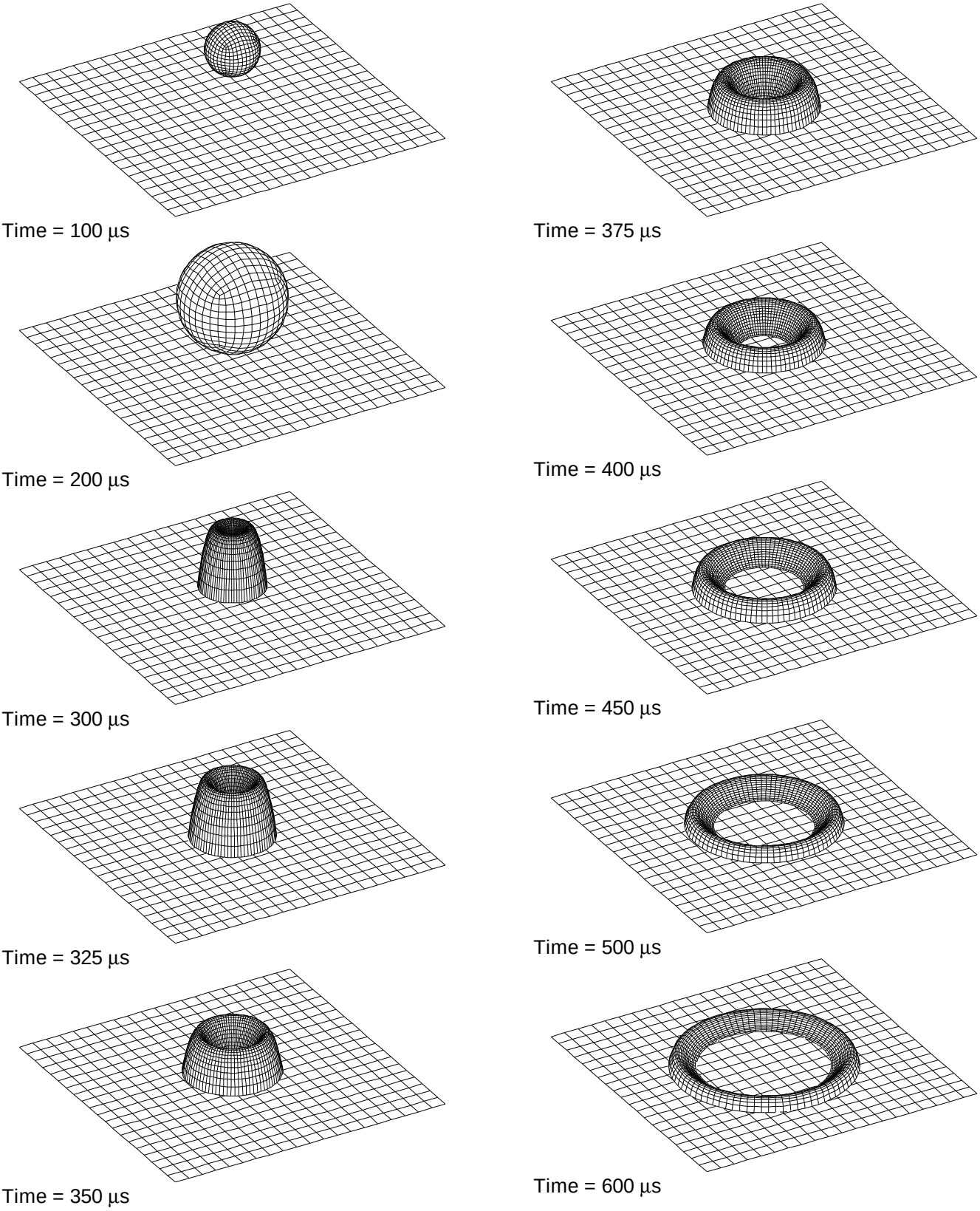

Figure 4. Gun Blast Pressure Wave Profiles

A pressure transducer placed on the panel will exhibit a history similar that shown in Figure 5. The pressure increases rapidly from zero to maximum and decays at a slower rate back to zero. Superimposed on this rise and decay is high frequency noise. The response frequency of the structure (100 - 500 Hz) is typically much lower than the excitation frequency of the pressure pulse (2-10 kHz). Therefore, panel response is governed by impulse (I) and this higher frequency noise is normally of little consequence.

Impulse is defined as

$$I = \int F(t)dt$$

Any pressure function which has a similar impulse to the blast pressure profile will generate similar response in the structure. Therefore, blast pressure may be simplified with the triangular shape shown in Figure 5.

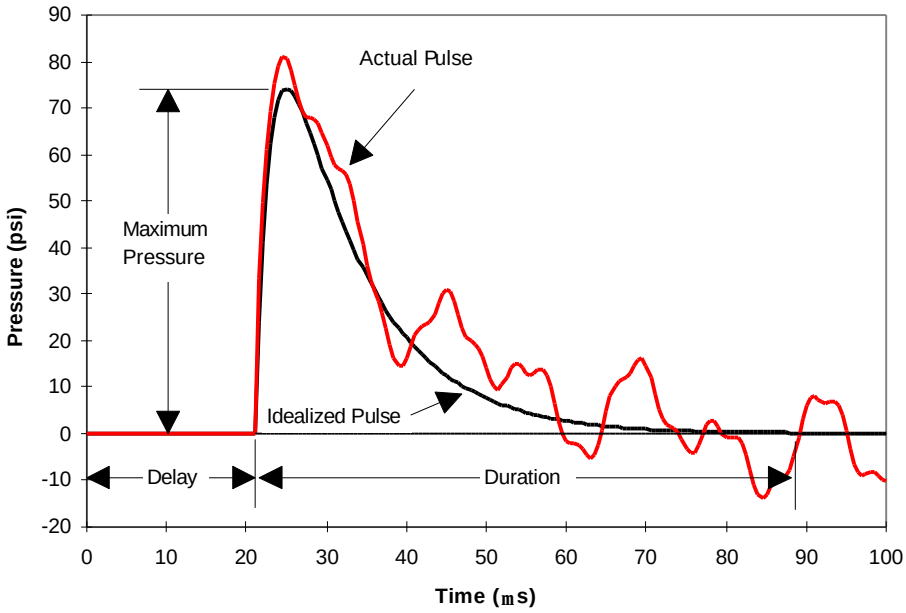

Figure 5. Gun Blast Pressure Pulse

Only three parameters are necessary using a triangular pressure model. These are delay to pressure wave arrival, duration of pressure wave, and maximum pressure. Using the NOL blast pressure model [4] these parameters are defined in terms of offset distance between the gun muzzle and the panel and the radial distance from the projected blast center as shown in Figure 6. Delay, duration, and maximum pressure for a sample blast are shown in Figures 7, 8, and 9, respectively.

A good understanding of the pressure wave from a particular gun is critical to developing analytical predictions. Therefore, pressure data from the 30 mm chain gun equipped with a muzzle brake were evaluated and fit with the NOL blast model. Blast pressure characteristics, corresponding to those shown Figures 7, 8, and 9, were then developed from limited available data for the 30mm cannon.

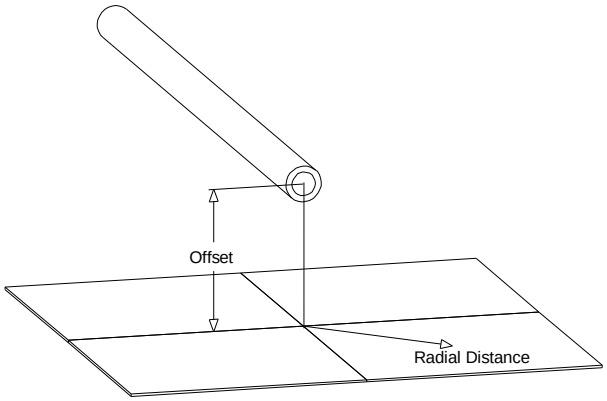

Figure 6. Gun Blast Pressure Pulse

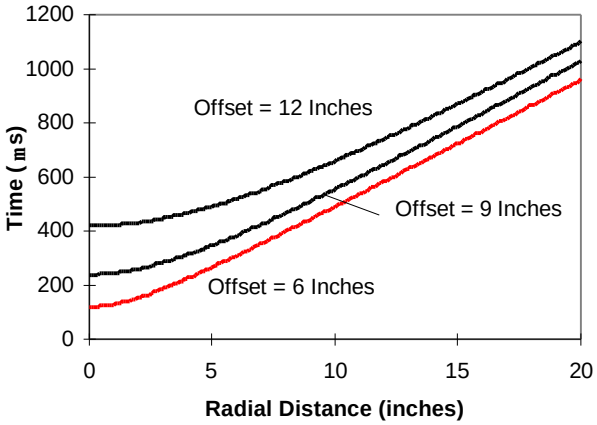

Figure 7. Gun Blast Pressure Pulse Delay

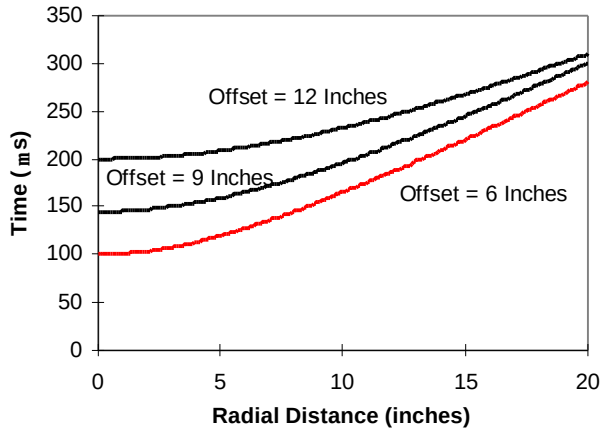

Figure 8. Gun Blast Pressure Pulse Duration

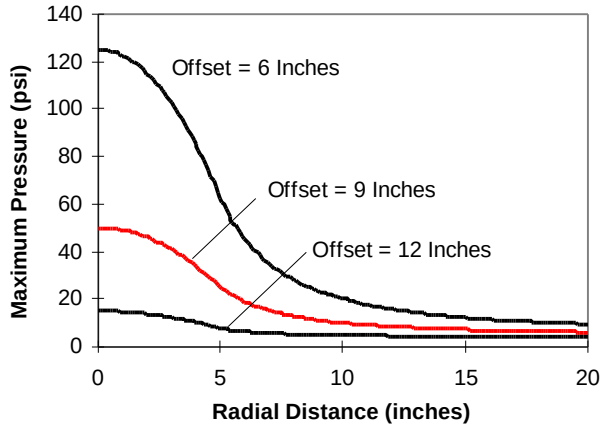

Figure 9. Gun Blast Peak Pressure Contours

ANALYSIS

The left lower EFAB skin, shown in Figure 10, was modeled with the finite element mesh shown in Figure 11. Skin, stringers, and longerons were modeled with linear quadratic shell elements. These elements were given anisotropic stiffness and mass properties corresponding to each lay-up. The panel was simply supported at the bulkhead with symmetrical boundary conditions at the centerline.

Each element in the skin exposed to the muzzle blast pressure wave was loaded with a transient triangular pressure pulse shown as in Figure 12. Each element has a pulse with a unique delay, duration, and maximum pressure depending on its proximity to the 30mm cannon muzzle.

This model was analyzed using NASTRAN Direct Transient Nonlinear Solution 129 on an HP C180 workstation. Deformations and maximum principal strains at 800 μs intervals are shown in Figure 13. Note that although the pressure wave has exited the panel in less than 1000 μs the panel deformation continues to increase to 3200 μs.

Strain gage time histories are shown in Figure 14 for the center of the skin, stringer, and longeron as shown in Figure 15. These strains are compared with material allowables to predict safety margins. The strains in the skin were sufficiently low such that the skin was softened in the final design (high ratio of +/-45 degree plies) to reduce the amount of load transferred to adjacent stringers and longeron.

Shear load history for the end of the center stringer is shown in Figure 16. This is the load transferred from the stinger to the longeron though an adhesive bond. Typically, structural failures from gun muzzle blast loading have occurred at interfaces between stringers and longerons [2]. Therefore, the transferred load was minimized by softening the stingers; and the load carrying capability was enhanced by increasing the bond footprint. These modifications were defined though analysis resulting in scalloped stiffeners used in the final design.

STRAIN GAGE CORRELATION

Prior to flight testing, little was known about the 30 mm gun blast pressure characteristics. Therefore, the center of one bay of the lower forward EFAB skin adjacent the gun muzzle was instrumented

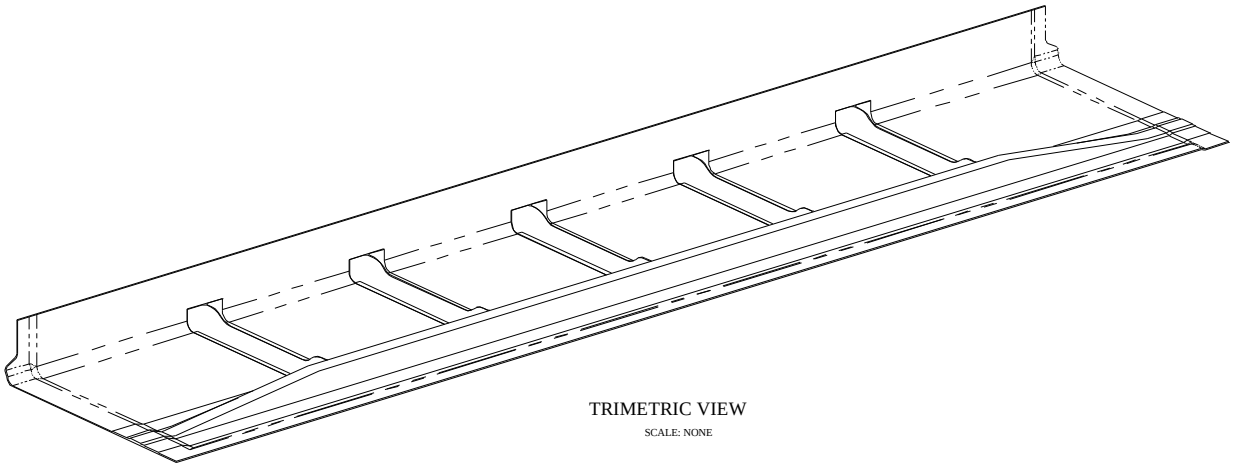

Figure 10. EFAB Lower Skin

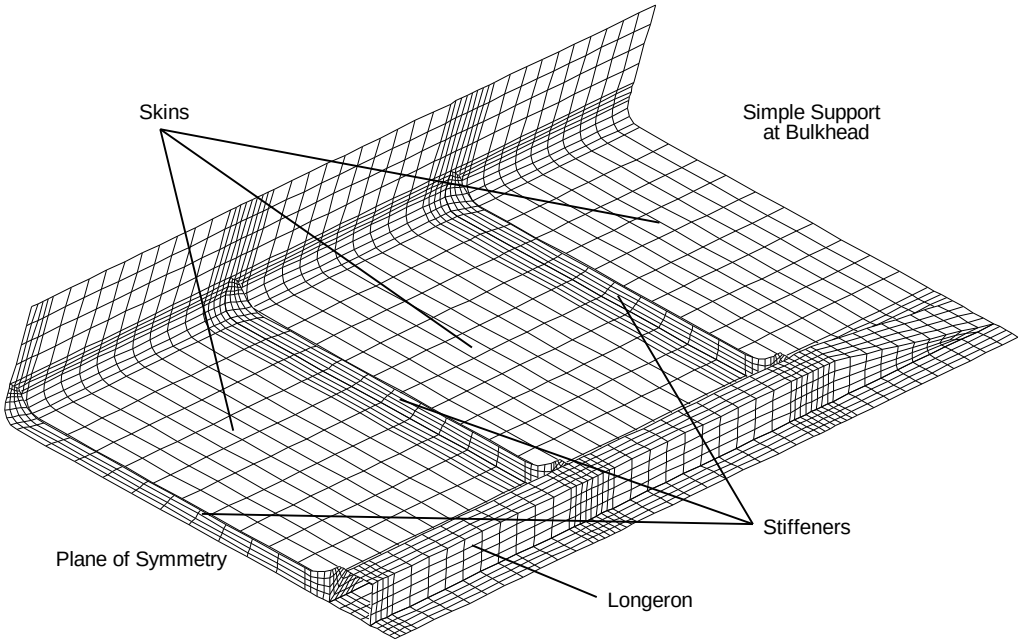

Figure 11. EFAB Lower Skin Finite Element Mesh

with a strain gage rosette, shown as Location 1 in Figure 15. Three channels of strain data were recorded for this rosette at 10 kHz during hover while the cannon was fired. Comparison of flight test to analytical strains indicated underprediction of extreme strains and overprediction of the duration of the first half wave of response.

Mass, simulating a small volume of displaced air, was removed and structural damping was reduced from 2% to .2% from the analytical model. No changes were made to the gun blast model. The analysis was rerun. The resulting analytical and measured strains are compared in Figures 17, 18, and 19 for lateral, longitudinal, and diagonal strain, respectively. There is good agreement between test and analysis for the first half wave of response both in response frequency and magnitude. This indicates that the blast pressure model used is sufficiently close to actual 30 mm chain gun blast characteristics.

The lack of agreement between test and analysis beyond the first half wave of response is due to the inability of this analytic model to accurately simulate damping and resonant wave interaction. Further investigation may be able to correct these deficiencies but is beyond the scope of this paper.

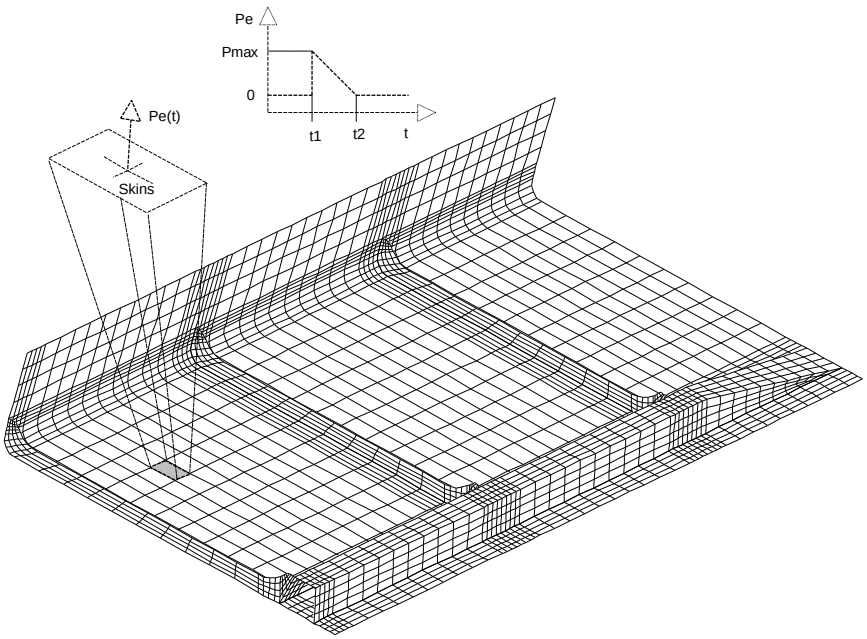

Figure 12. Element Pressure Pulse Simulation

RECOMMENDATIONS AND CONCLUSION

It is critical for accurate analytical predictions to obtain pressure maps and time histories for muzzle blast from a particular gun. This data should then be fit to the NOL blast pressure model to obtain duration, delay, and maximum pressure as a function of location for each exposed element in a finite element model.

Models should be analyzed using geometric non-linearity to capture deformation hardening (and softening) of pressurized skins. Use the minimum damping necessary to obtain solution convergence. Use large safety factors (>2.0) when sizing structure due to uncertainties in blast pressure characteristics and structure dynamic behavior.

Structure subjected to gun muzzle blast should be as compliant as possible while maintaining structural integrity to minimize transferred loads. Internal shear joints require special attention to ensure adequate strength for transferred loads.

The analysis method presented resulted in a light weight composite structure capable of withstanding 30 mm chain gun muzzle pressure loads. Data obtained during flight test verified the blast pressure model, the analysis methodology, as well as structural integrity of the design.

REFERENCES

1. Dobyns, A. L., McCarthy, D. K., Hong, S. W., “Muzzle Blast Response of Metal and Composite Structures,” Proceedings of the 1987 SEM Fall Conference - DYNAMIC FAILURE, October, 1987.

2. Dobyns, A. L., Boyce, W., McCarthy, D. K., Urban, M. R., “Advanced Composite Airframe Program - Airframe Weapons Interface,” USAAVSCOM TR-89-D-1, US Army AATD, July, 1989.

3. McCarthy, D. K., Dobyns, A. L., “ The Analysis and Testing of Composite Panels Subject to Muzzle Blast Effects,” Proceedings of the American Helicopter Society National Technical Specialists’ Meeting - Fatigue Methodology III, October, 1989.

4. Proctor, J. F., “Internal Blast Damage Mechanisms Computer Program,” NOLTR-72-231, Naval Ordnance Laboratory, Silver Spring, MD, August, 1972.

5. Dobyns, A. L., “Fiber Composite-Blast Response Computer Program (BR1-FC) BR-1 Code Modification and Test Program,” AFFDL-TR-78-29, October 1977.

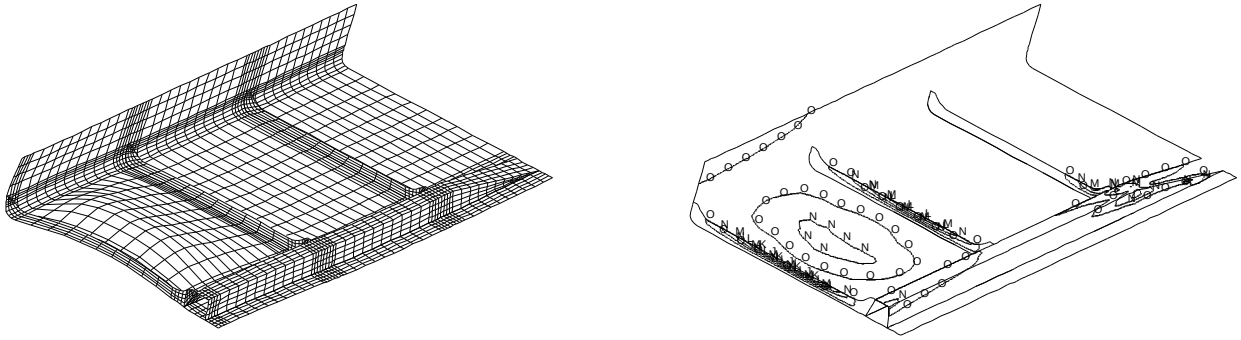

Deformed shape and strain at time = 800 μs

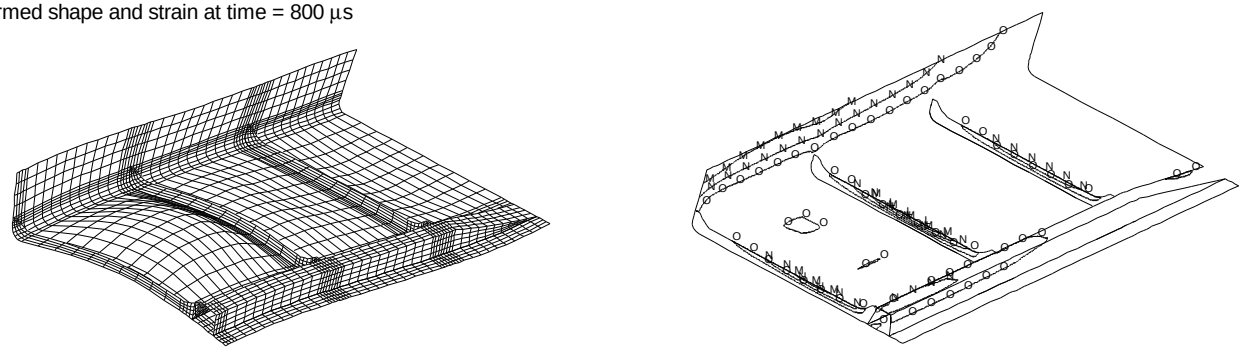

Deformed shape and strain at time = 1600 μs

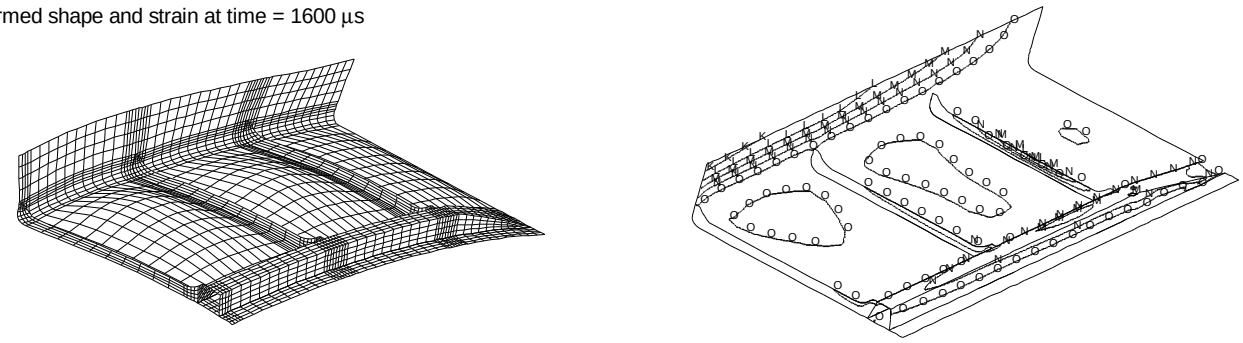

Deformed shape and strain at time = 2400 μs

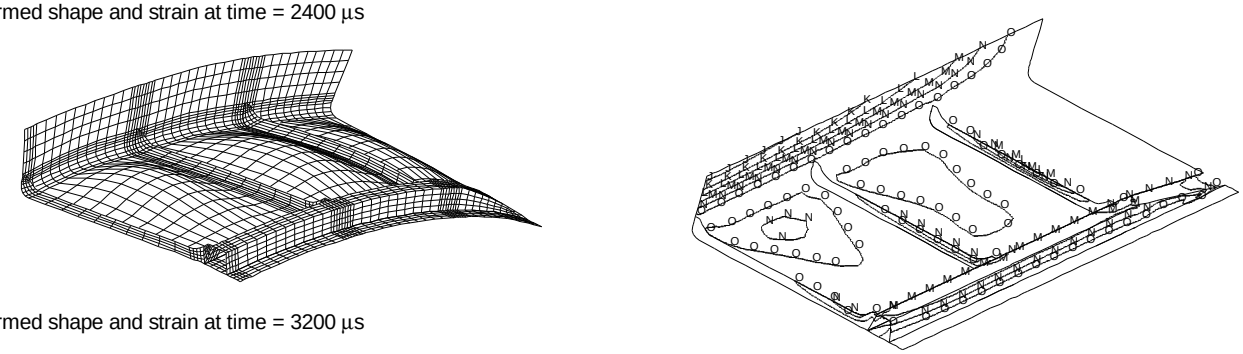

Deformed shape and strain at time = 3200 μs

A	=	6000	με		F	=	4000	με		K	=	2000	με
B	=	5600	με		G	=	3600	με		L	=	1600	με
C	=	5200	με		H	=	3200	με		M	=	1200	με
D	=	4800	με		I	=	2800	με		N	=	800	με
E	=	4400	με		J	=	2400	με		O	=	400	με

Figure 13. EFAB Lower Skin FE Maximum Principal Strain and Displacement Results

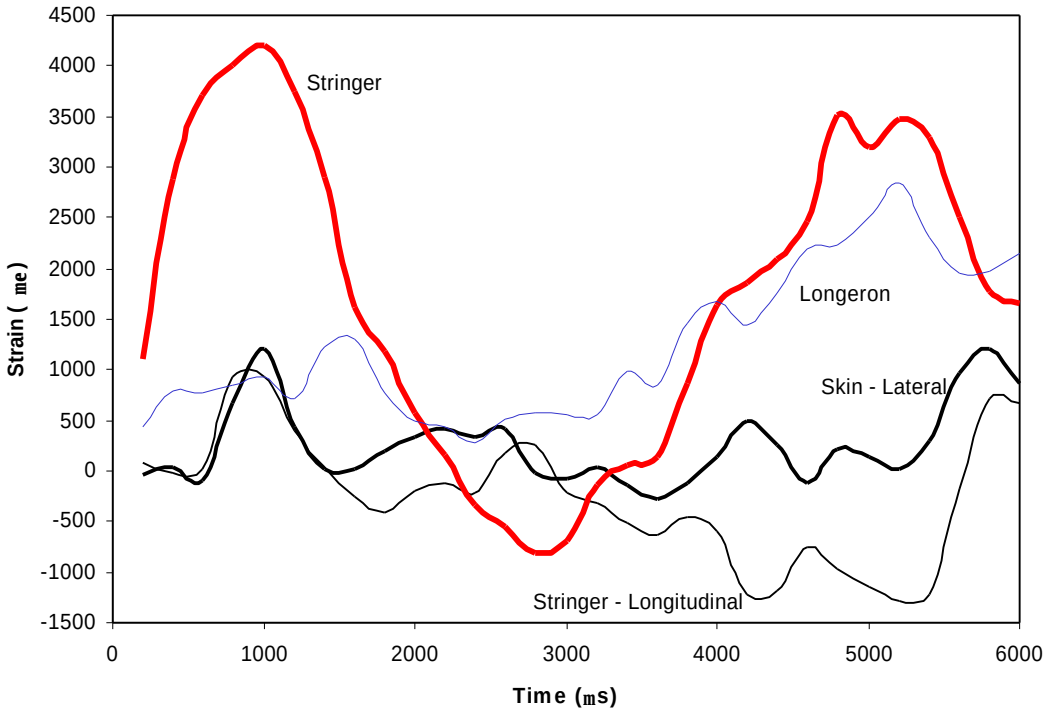

Figure 14. EFAB Lower Skin Strain Histories

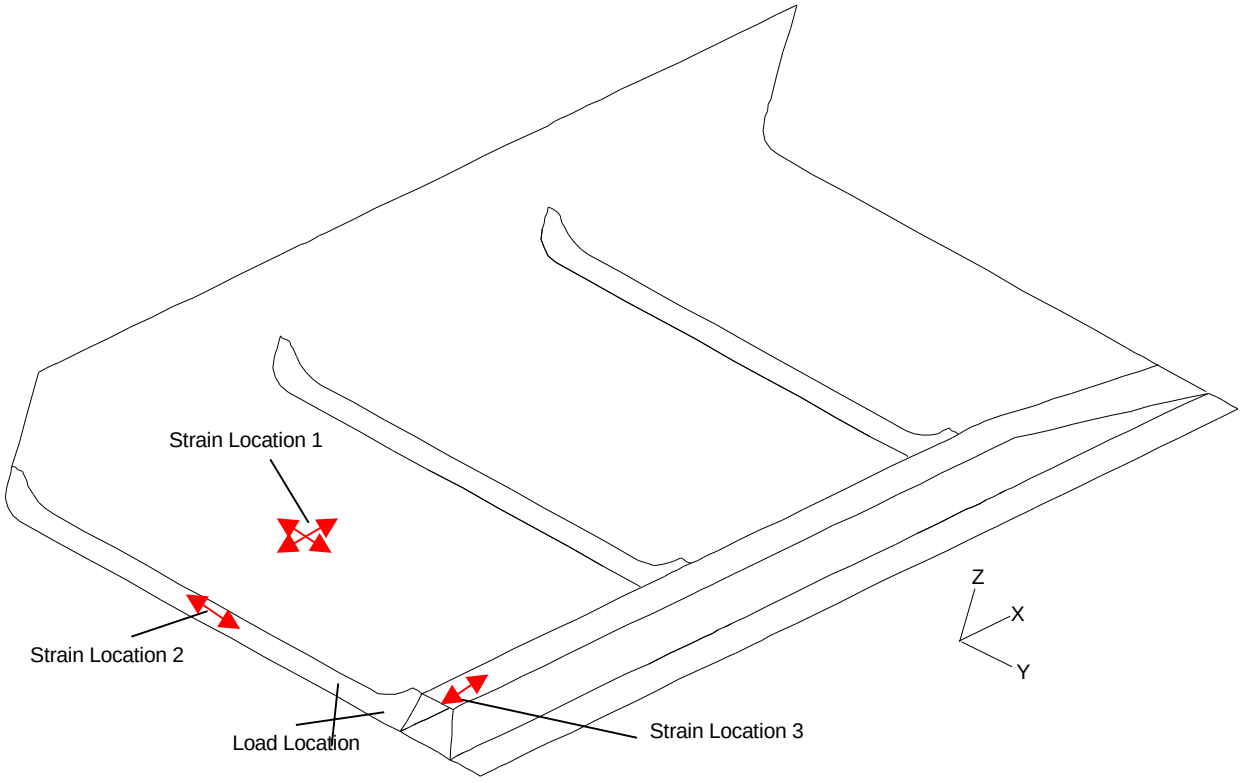

Figure 15. EFAB Lower Skin Finite Element Model

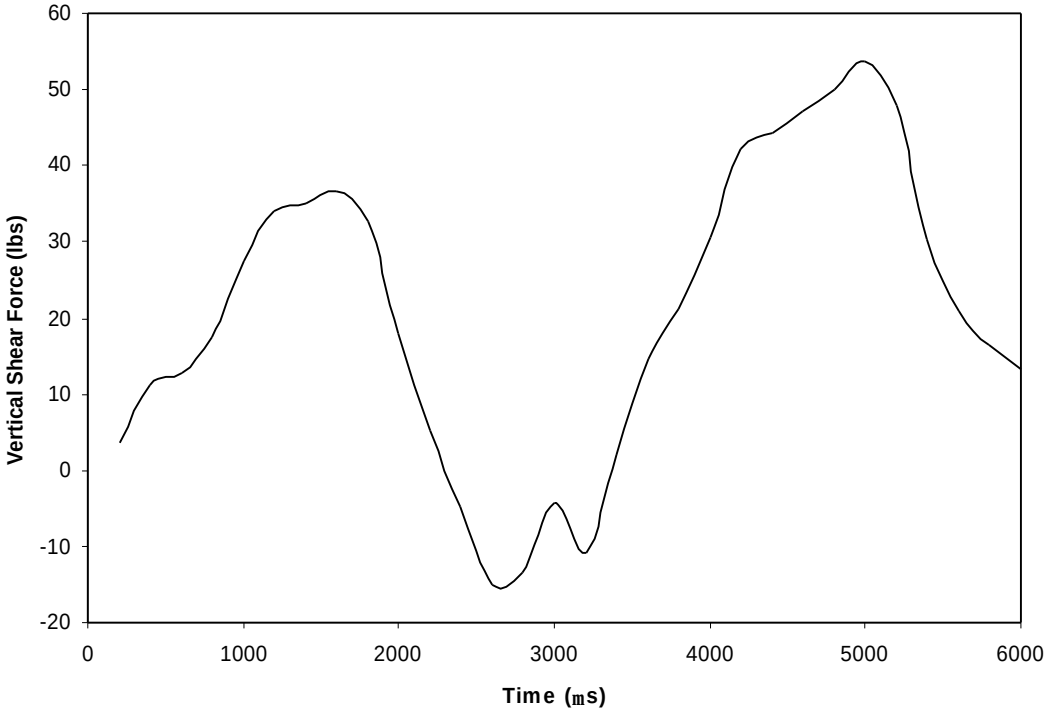

Figure 16. EFAB Lower Skin Stringer Load History

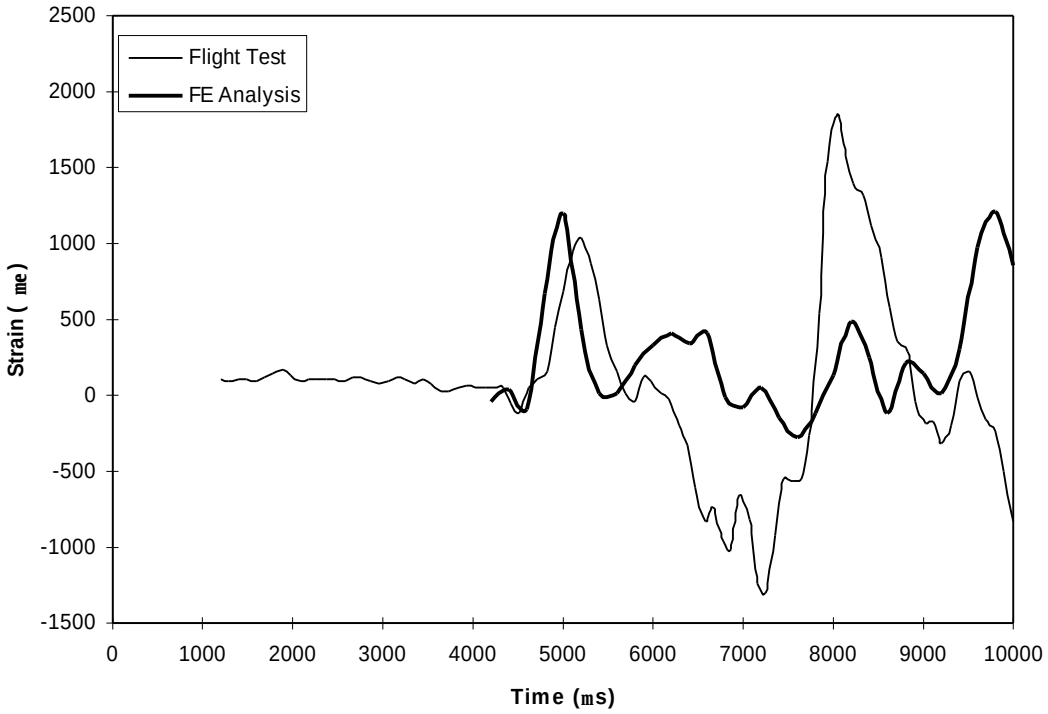

Figure 17. EFAB Lower Skin Lateral Strain Correlation

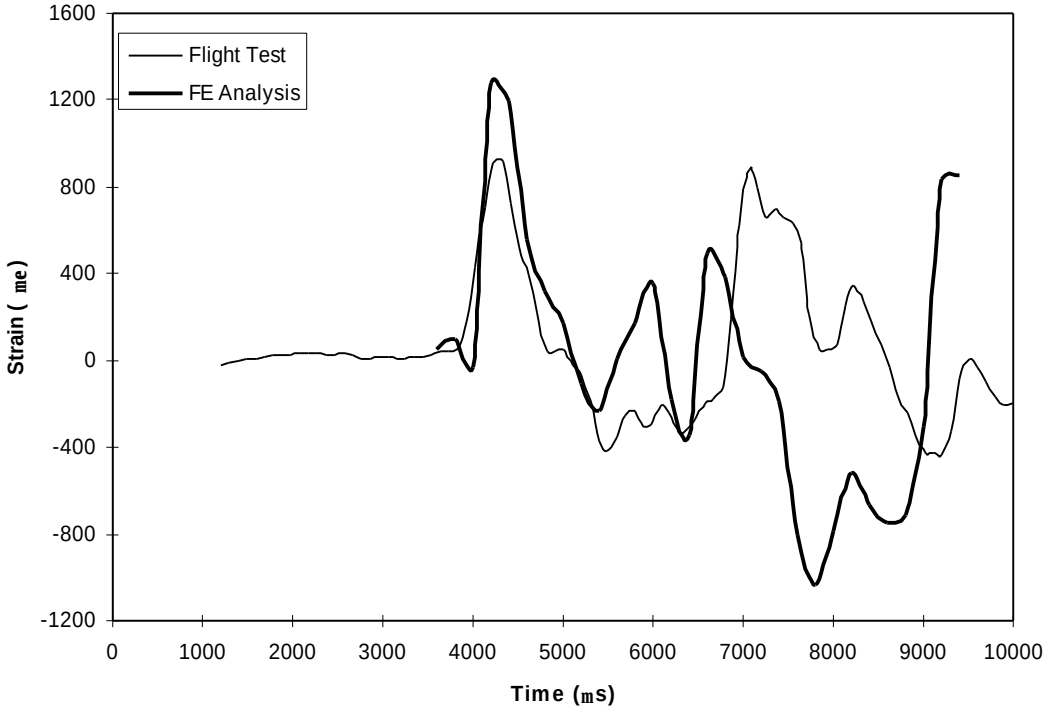

Figure 18. EFAB Lower Skin Diagonal Strain Correlation

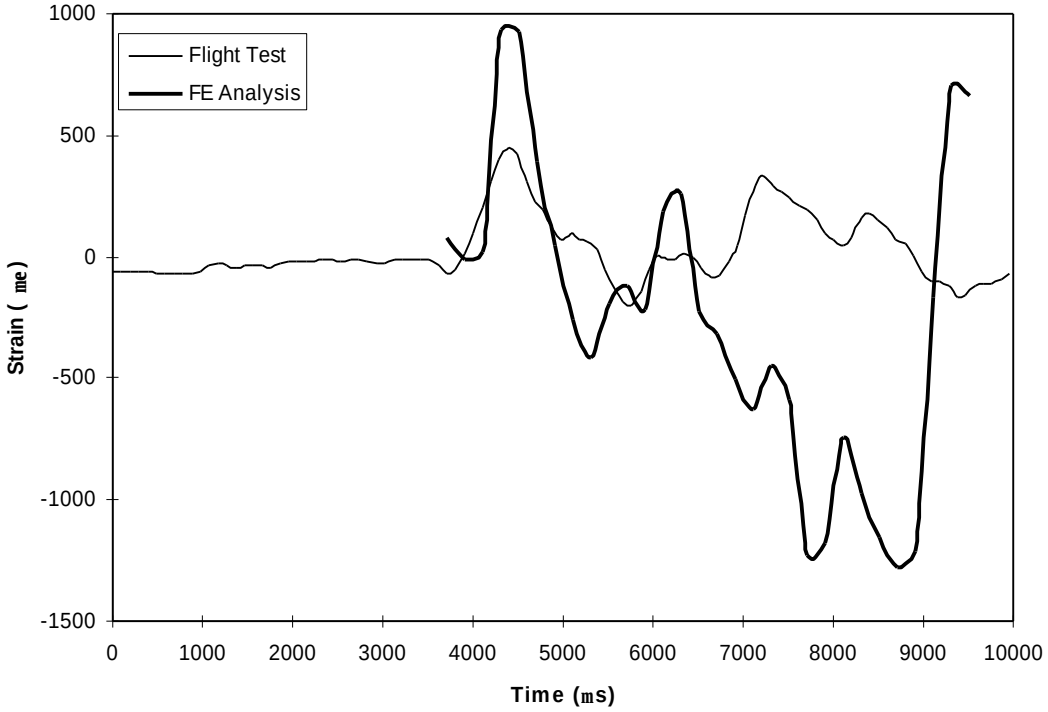

Figure 19. EFAB Lower Skin Longitudinal Strain Correlation